

Structure, phase behavior and inhomogeneous fluid properties of binary dendrimer mixtures

I. O. Götze,¹ A. J. Archer,² and C. N. Likos¹

¹*Institut für Theoretische Physik II, Heinrich-Heine-Universität Düsseldorf,
Universitätsstraße 1, D-40225 Düsseldorf, Germany*

²*H. H. Wills Physics Laboratory, University of Bristol, Bristol BS8 1TL, UK*
(Dated: June 14, 2021)

The effective pair potentials between different kinds of dendrimers in solution can be well approximated by appropriate Gaussian functions. We find that in binary dendrimer mixtures the range and strength of the effective interactions depend strongly upon the specific dendrimer architecture. We consider two different types of dendrimer mixtures, employing the Gaussian effective pair potentials, to determine the bulk fluid structure and phase behavior. Using a simple mean field density functional theory (DFT) we find good agreement between theory and simulation results for the bulk fluid structure. Depending on the mixture, we find bulk fluid-fluid phase separation (macro-phase separation) or micro-phase separation, i.e., a transition to a state characterized by undamped periodic concentration fluctuations. We also determine the inhomogeneous fluid structure for confinement in spherical cavities. Again, we find good agreement between the DFT and simulation results. For the dendrimer mixture exhibiting micro-phase separation, we observe rather striking pattern formation under confinement.

PACS numbers: 61.25.Hq, 82.70.Dd, 36.20.Ey, 61.12.Ex

I. INTRODUCTION

Dendrimers are highly branched polymeric macromolecules. They are synthesized from monomers that can form bonds with at least three other monomers. Starting from a suitable central molecule, a number of generations of monomers are sequentially added. With the addition of each successive generation, the dendrimer becomes increasingly branched in its internal structure.^{1,2,3,4,5} A dendrimer with n generations of monomers is denoted a G_n dendrimer. Dendrimers have numerous technological applications – for example in the targeted delivery of drugs^{6,7} and, in particular, anti-cancer agents,^{8,9,10} in light-harvesting applications,¹¹ and also as a tool for the development of nonviral gene delivery.¹² In a dendrimer solution, the individual macromolecules feature different conformations due to fluctuations of the monomers. However, statistically one finds that the intra-molecular monomer distribution is almost spherically symmetric. For the statistical behavior of the ensemble of macromolecules only the average over all conformations and orientations of the interacting dendrimers has to be taken into account, provided no phases with orientational order appear. This suggests treating the interaction between dendrimers via radially symmetric effective pair potentials, even though a dendrimer is a complex, structured object. Also, given the number of degrees of freedom in each dendrimer, determining the structure and phase behavior of suspensions of dendrimers starting from an atomistic view point is a tough problem. Obtaining an effective interaction potential between pairs of dendrimers (e.g. between the centres of mass) is a way to surmount this. In such a procedure, one is effectively integrating in the partition function over the internal monomeric degrees of freedom of each dendrimer, resulting in an effective

Hamiltonian for the dendrimer mixture that treats each dendrimer as a point particle.^{13,14,15,16,17} However, in principle such an effective Hamiltonian also includes effective three-body and higher body effective interactions between the particles.^{13,17} For dendrimers in solution one finds that these three and higher body interactions are small compared to the two-body potentials,¹⁷ so neglecting these higher body terms in the effective Hamiltonian is justified. Given an effective Hamiltonian for point particles one can then determine the fluid structure and phase behavior by means of theory or simulations. Thus, effective interactions are a powerful tool to bridge the length scales and to extract macroscopic properties of dendrimer solutions from microscopic details.

In this paper we use such an approach to study binary dendrimer mixtures. We find that all effective pair potentials between dendrimers take a Gaussian form.^{14,18} The parameters in these potentials depend strongly on the specific dendrimer architectures, to the extent that we can ‘tune’ their range and strength by changing the number of generations and flexibility between monomers in the dendrimers. This enables us to study the occurrence of a number of phenomena that have been predicted for Gaussian mixtures, such as bulk fluid-fluid demixing^{19,20} and micro-phase separation.²¹ Micro-phase separation²² is characterized by a transition in the fluid to a state with undamped periodic concentration fluctuations which is thought to indicate a thermodynamic transition to a rather unusual crystalline state.²¹ When Gaussian mixtures are subject to geometrical confinement, pattern formation can spontaneously arise.²¹ We find dendrimer mixtures exhibiting all these phenomena. Thus, we are able to demonstrate that the rich phenomenology encountered in Gaussian mixtures corresponds to *real* systems.

This paper is laid out as follows: In Sec. II we describe our procedure for determining the effective pair potentials in dendrimer mixtures and give results for two particular systems. In Sec. III we briefly describe theories that apply for Gaussian mixtures and then in Sec. IV we present theory and simulation results for the bulk structure and phase behavior of particular dendrimer mixtures. In Sec. V we present theory and simulation results for two particular dendrimer mixtures confined in spherical cavities. Finally, in Sec. VI we draw our conclusions.

II. EFFECTIVE PAIR POTENTIALS

It has been shown by means of monomer-resolved simulations and theory, that the effective pair potentials between the centres of mass of dendrimers in a good solvent can be modelled by a purely repulsive Gaussian potential of the form:¹⁴ $V(r) = \epsilon \exp(-r^2/R^2)$, where the parameters $\epsilon > 0$ and R depend strongly upon the parameters characterizing the dendrimer's specific architecture. In particular, they are both affected by the terminal generation number and the bond length between successive generations. It is therefore possible to 'tune' the effective interactions by modifying these parameters. This result has also been confirmed by making comparison with experimental results.¹⁵ In the present work we determine the effective pair potential between *different* types of dendrimers. We find that in binary mixtures, these can also be well approximated by Gaussian functions of different ranges and strengths. The pair potential between two dendrimers of species i and j thus takes the form:

$$V_{ij}(r) = \epsilon_{ij} \exp(-r^2/R_{ij}^2), \quad (1)$$

where the parameters $\epsilon_{ij} > 0$ and R_{ij} depend strongly on the specific properties of the two types of dendrimers in question.

In order to obtain the effective interaction potentials between a pair of dendrimers, we employed a simple coarse-grained model, the so-called bead-thread model,¹⁶ which treats the monomers as hard spheres of diameter σ , connected by ideal threads of maximum extension $(1 + \delta)\sigma$. The parameter δ corresponds to the length of the polymer chains between two branching points in the dendrimer. Increasing the number of chemical bonds between two branching points leads to an increase in flexibility of the polymer and thus to softer but more long ranged effective interactions between dendrimers. Large values of δ are used to model dendrimers with open structures and compact dendrimers are modelled by choosing a smaller value of δ . As the number of generations (monomers) is increased, the radius of the molecule, of course, increases and the average monomer density inside the molecule grows as well. For a fixed number of monomers in the dendrimer, the value of the effective pair potential for complete overlap of the centres of mass of a pair of dendrimers decreases upon increasing δ . Upon increasing the generation number G , keeping

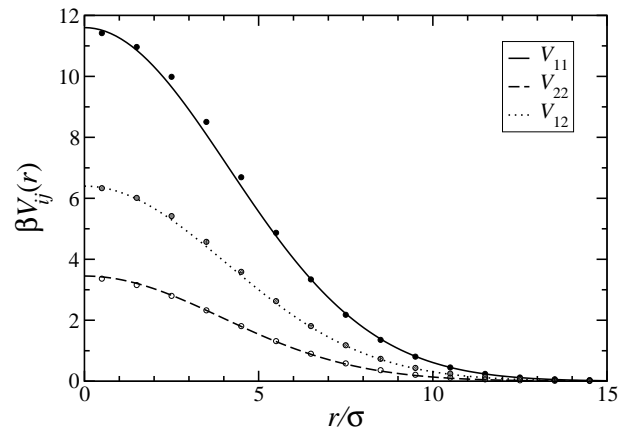


FIG. 1: Effective pair potentials $V_{ij}(r)$ between dendrimers in a binary mixture exhibiting macro-phase separation (system A). Species 1 is a G4 dendrimers with $\delta = 2.0\sigma$ and species 2 is a G3 dendrimers with $\delta = 3.0\sigma$. The corresponding MC data are shown as circles.

δ fixed, the effective interaction becomes more repulsive because of the exponential growth of the monomer number with G . By varying δ and G , one can easily modify the dendrimer architecture and thereby systematically 'tune' the effective pair potential between dendrimers of the same kind.¹⁴ However, it is much less straightforward to a priori determine the cross-interaction between two dendrimers with different values for the parameters δ and G . At the same time, employing mixtures of different dendrimer types dramatically increases the freedom to tailor the macroscopic properties of the system.

To determine effective dendrimer interactions $V_{ij}(r)$, $i, j = 1, 2$ in a binary mixture, we employ monomer-resolved Monte-Carlo (MC) simulations of the bead-thread model for dendrimers of different generations and varying thread length δ . We simulate pairs of dendrimers of species i and j and determine in the simulation the probability $P_{ij}(r)$ of finding their centers of mass separated by distance r . Thereafter, the effective potential $V_{ij}(r)$ can be obtained using the relation:

$$\beta V_{ij}(r) = -\ln[g_{ij}(r)], \quad (2)$$

where $\beta = 1/k_B T$ is the inverse temperature and $g_{ij}(r) \propto P_{ij}(r)$, are the partial radial distribution functions.¹³ Due to the strong repulsion for complete overlap between dendrimers, we use biased MC, as described in Ref. 14, to obtain the effective potentials. The MC-results for $V_{ij}(r)$ can be very well described by Gaussian functions of the form in Eq. (1), as can be seen in Figs. 1 and 2.

Having derived effective Gaussian pair potentials for a given binary dendrimer mixture it is then possible to apply theories developed for point particles to calculate the mixture structure and thermodynamics. Such a theory is described in the next section. Typically, we find that most binary dendrimer mixtures exhibit bulk fluid-fluid

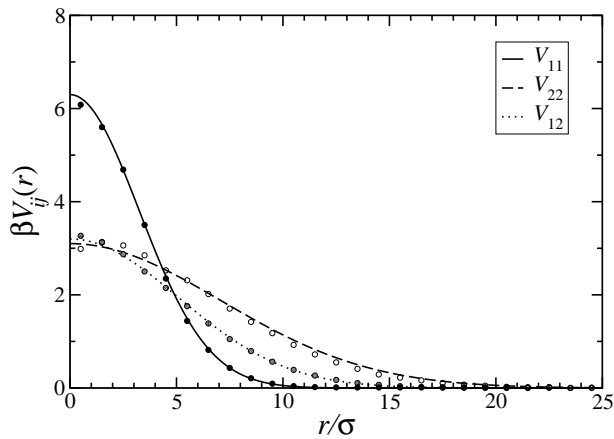


FIG. 2: Effective pair potentials $V_{ij}(r)$ between dendrimers in a binary mixture exhibiting micro-phase separation (system B). Species 1 is a G3 dendrimers with $\delta = 2.0\sigma$ and species 2 is a G4 dendrimers with $\delta = 4.7\sigma$. The corresponding MC data are shown as circles.

phase separation (macro-phase separation). In Fig. 1 we display the effective pair potentials for a particular binary mixture that does exhibit macro-phase separation. This mixture is composed of G4 dendrimers with $\delta = 2.0\sigma$ together with G3 dendrimers with $\delta = 3.0\sigma$. However, in one particular mixture that we investigated, we find that the mixture exhibits micro-phase separation.²¹ This mixture is composed of G3 dendrimers with $\delta = 2.0\sigma$ together with G4 dendrimers with $\delta = 4.7\sigma$. The effective pair potentials for this mixture are displayed in Fig. 2. It can be seen there that the key ingredient for generating micro-phase separation is that the effective potentials in one species are short-ranged and strongly repulsive, whilst the effective interactions in the other species are long-ranged with soft repulsion.

III. THEORY

Having derived effective pair potentials between the different species of dendrimers in a particular binary mixture, we now use these potentials as input to liquid state theories developed for determining the fluid structure and thermodynamics. It has been shown that a simple mean field DFT which generates the random phase approximation (RPA) for the fluid direct pair correlation functions²³ provides an accurate description of the bulk and inhomogeneous structure of fluids composed of Gaussian particles,^{18,19,20} and more generally, for fluids composed of particles interacting via bounded or even weakly diverging soft potentials.^{25,26,27} The intrinsic Helmholtz free energy functional of the inhomogeneous mixture is given by:

$$\mathcal{F}[\{\rho_i\}] = \mathcal{F}_{\text{id}}[\{\rho_i\}] + \mathcal{F}_{\text{ex}}[\{\rho_i\}], \quad (3)$$

where

$$\mathcal{F}_{\text{id}}[\{\rho_i(\mathbf{r})\}] = k_B T \sum_i \int d\mathbf{r} \rho_i(\mathbf{r}) [\ln(\Lambda_i^3 \rho_i(\mathbf{r})) - 1], \quad (4)$$

is the (exact) ideal gas contribution to the free energy²³ and Λ_i is the thermal de Broglie wavelength for the dendrimers of species i . The quantity $\mathcal{F}_{\text{ex}}[\{\rho_i\}]$ is the excess (over ideal) contribution to the free energy due to interactions between the particles. The RPA approximation for this quantity is

$$\mathcal{F}_{\text{ex}}[\{\rho_i\}] = \frac{1}{2} \sum_{ij} \int d\mathbf{r}_1 \int d\mathbf{r}_2 \rho_i(\mathbf{r}_1) \rho_j(\mathbf{r}_2) V_{ij}(|\mathbf{r}_1 - \mathbf{r}_2|). \quad (5)$$

The fluid direct pair correlation functions generated by the RPA functional are simply,²³

$$c_{ij}^{(2)}(\mathbf{r}_1, \mathbf{r}_2) \equiv -\frac{\beta \delta^2 \mathcal{F}_{\text{ex}}}{\delta \rho_i(\mathbf{r}_1) \delta \rho_j(\mathbf{r}_2)} = -\beta V_{ij}(|\mathbf{r}_1 - \mathbf{r}_2|). \quad (6)$$

For a given set of one body external potentials $\{V_i^{\text{ext}}(\mathbf{r})\}$, the fluid one body density profiles are obtained by minimising the grand potential functional:^{21,23}

$$\Omega[\{\rho_i\}] = \mathcal{F}[\{\rho_i\}] - \sum_{i=1}^2 \int d\mathbf{r} (\mu_i - V_i^{\text{ext}}(\mathbf{r})) \rho_i(\mathbf{r}), \quad (7)$$

where μ_i is the chemical potential for species i .

Given such a DFT, one can calculate the fluid partial radial distribution functions $g_{ij}(r)$ using the so called ‘test-particle route’, in which one fixes a particle of species j and then calculates the fluid one-body density profiles around this fixed particle – i.e. one sets the external potentials in Eq. (7) equal to the fluid pair potentials. The partial radial distribution function are then given by $g_{ij}(r) = \rho_i(r)/\rho_i^b$, where ρ_i^b is the bulk fluid density of species i .

An alternative route to determining the bulk fluid structure is via the Ornstein-Zernike (OZ) equations.²⁴ In Fourier space, the OZ equations for a two-component fluid take the form

$$\hat{h}_{ij}(q) = \frac{N_{ij}(q)}{D(q)}, \quad (8)$$

where $\hat{h}_{ij}(q)$ is the (3 dimensional) Fourier transform (FT) of $h_{ij}(r) = g_{ij}(r) - 1$ and the numerator functions are

$$\begin{aligned} N_{11}(q) &= \hat{c}_{11}(q) + \rho_2^b [\hat{c}_{12}^2(q) - \hat{c}_{11}(q) \hat{c}_{22}(q)], \\ N_{22}(q) &= \hat{c}_{22}(q) + \rho_1^b [\hat{c}_{12}^2(q) - \hat{c}_{11}(q) \hat{c}_{22}(q)], \\ N_{12}(q) &= \hat{c}_{12}(q), \end{aligned} \quad (9)$$

and the denominator

$$D(q) = [1 - \rho_1^b \hat{c}_{11}(q)][1 - \rho_2^b \hat{c}_{22}(q)] - \rho_1^b \rho_2^b \hat{c}_{12}^2(q), \quad (10)$$

where $\hat{c}_{ij}(q)$ is the FT of the bulk direct pair correlation function $c_{ij}(r)$.²⁰ We define the fluid partial structure factors as follows:

$$S_{ij}(q) = \delta_{ij} + \sqrt{\rho_i^b \rho_j^b} \hat{h}_{ij}(q). \quad (11)$$

In Sec. IV we display some typical results for the fluid partial radial distribution functions and structure factors. However, before discussing results for specific systems, we remind the reader of some basic connections between fluid structure and phase behavior.

Given an expression for the Helmholtz free energy functional for a fluid, it is then straight forward to calculate the bulk fluid phase behavior. The Helmholtz free energy F for the bulk fluid is simply obtained by substituting $\rho_i(\mathbf{r}) = \rho_i^b$ into $\mathcal{F}[\{\rho_i\}]$ and the pressure P follows as $P = -(\partial F/\partial V)_{N_1, N_2, T}$, where V is the volume of the system. Through a Legendre transformation, the Gibbs free energy $G(N_1, N_2, P, T) = F(N_1, N_2, V, T) + PV$ is obtained, along with the intensive Gibbs free energy per particle, $G/N \equiv g(x, P, T)$, where $x = N_2/N$ and $N = N_1 + N_2$. If, at fixed P and T , $g(x, P, T)$ is a convex function of x ($g''(x) > 0$) for all x -values, the homogeneous mixture is stable. If, on the other hand, there are parts with $g''(x) \leq 0$, then the system exhibits bulk fluid-fluid phase separation and the coexisting state points are obtained by equating the pressure and chemical potentials in the coexisting phases.²⁰ Within mean field (van der Waals-like) theories such as the present, a fluid-fluid coexistence curve (binodal) is always accompanied by a spinodal which is the locus in the phase diagram where the inverse isothermal compressibility $\chi_T^{-1} = 0$, - i.e. the locus of points at which $(\partial^2 g/\partial x^2)_{P, T} = 0$. The compressibility χ_T is simply related to the $q = 0$ value of the fluid static structure factor $S(q)$,²⁴ so the spinodal can equally be defined as the locus in the phase diagram at which $S(q = 0) \rightarrow \infty$. $S(q)$ can be expressed as a linear combination of the partial structure factors^{24,30} in Eq. (11), i.e., as a linear combination of the functions $\hat{h}_{ij}(q)$. From Eq. (8) we see that the spinodal is given by the locus in the phase diagram of $D(q = 0) = 0$. Using the RPA approximation $c_{ij}(r) = -\beta V_{ij}(r)$ in Eq. (10), we obtain an analytic expression for $D(q)$ and thus we have a simple way of determining if a particular dendrimer mixture has a spinodal and therefore exhibits bulk fluid-fluid phase separation.²⁰

In addition to exhibiting macro-phase separation, binary mixtures of Gaussian particles are capable of exhibiting micro-phase separation.²¹ This occurs when at a wavenumber $q = q_c > 0$, there is a divergence $S(q_c) \rightarrow \infty$ (and therefore also a divergence in $S_{ij}(q)$ at $q = q_c$). This is equivalent to $D(q_c) \rightarrow 0$. We define the λ -line as the locus in the phase diagram at which $D(q \neq 0) = 0$. This line has a U-shape and separates the (ρ, x) -plane into two regions. Below the λ -line $D(q) > 0$ for all q values,²¹ whereas above it the uniform fluid mixture is unstable. Using the RPA approximation in Eq. (10) it is simple to locate the λ -line for mixtures exhibiting micro-phase separation.

IV. BULK RESULTS

In this section, we display results for the bulk structure and phase behavior of two particular binary mixtures of dendrimers, the first of which exhibits bulk fluid-fluid phase separation (macro-phase separation) and the second exhibits micro-phase separation. In both these systems the macro-phase separation (in the former) and the micro-phase separation (in the latter) occur at fluid densities sufficiently high as to make simulating these systems near to phase separation computationally expensive, particularly since close to the spinodal/ λ -line, bulk simulations become impractical due to the long-range nature of the fluid correlation functions, requiring very large simulation systems to obtain reliable results. Thus, we compare results from the RPA DFT with simulations at lower densities, in order to evaluate the reliability of the theory. Given that the accuracy of the RPA approximation improves with increasing density,^{13,18,26} the good agreement between theory and simulations that we find at lower densities implies that the RPA is reliable for determining the phase behavior of Gaussian mixtures at higher densities. In our simulation results, we excluded finite size effects by performing simulations at the same density but different total numbers of dendrimers (20 000 and 100 000), that both yield identical results.

A. Macro-phase separation

The first system we investigate, hereafter referred to as ‘system A’, consists of G4 dendrimers with $\delta = 2.0\sigma$ (in the following termed species 1), and G3 dendrimers with $\delta = 3.0\sigma$ (species 2). In this mixture the ranges of the interaction potentials R_{ij} are all very similar, but they differ markedly in the prefactors ϵ_{ij} . The parameters of the effective pair potentials in Eq. (1) for system A are:

$$\begin{aligned} \epsilon_{11} &= 11.6 k_B T, & R_{11} &= \sqrt{34}\sigma \\ \epsilon_{22} &= 3.45 k_B T, & R_{22} &= \sqrt{31}\sigma \\ \epsilon_{12} &= 6.4 k_B T, & R_{12} &= \sqrt{33}\sigma. \end{aligned}$$

The pair potentials with these parameters are plotted in Fig. 1. The radial distribution functions $g_{ij}(r)$ for system A are displayed in Fig. 3 for the total bulk density $\rho R_{11}^3 = (\rho_1^b + \rho_2^b) R_{11}^3 = 1.49$ and concentration $x = \rho_2^b/\rho = 0.5$. We plot MC simulation results, results obtained by inserting the RPA closure into the OZ equations and those from using the RPA DFT via the test-particle route. The latter route guarantees $g_{ij}(r) > 0$ and is much more reliable than the RPA OZ route. Nonetheless, the RPA OZ results still agree well with the simulations results for $r > R_{11}$. It is at small r where deviations and even unphysical negative values of $g_{ij}(r)$ appear in the RPA OZ results at lower total densities ρ .

In Fig. 4 we display the partial structure factors $S_{ij}(q)$ for system A at the state point corresponding to the results displayed in Fig. 3. We see a peak in the struc-

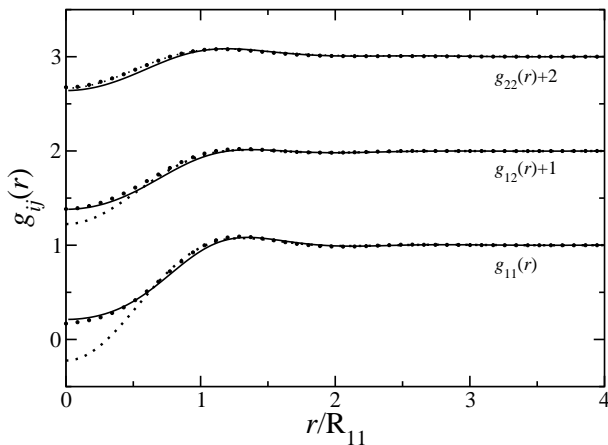


FIG. 3: Partial radial distribution functions $g_{ij}(r)$ for system A with a total density $\rho R_{11}^3 = 1.49$ and concentration $x = 0.5$. The circles are MC simulation results, the solid lines DFT test-particle results and the dotted lines results from the RPA closure to the OZ equations.

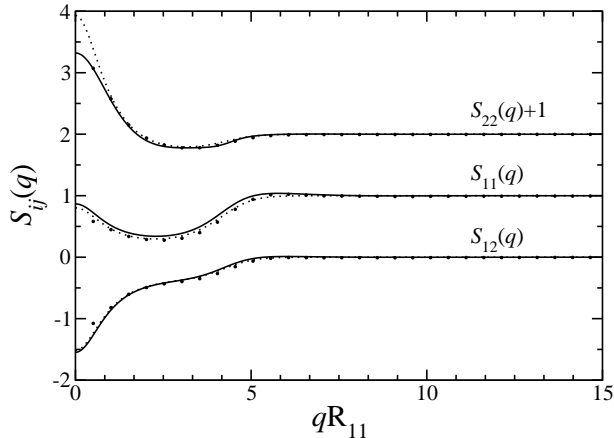


FIG. 4: Partial structure factors $S_{ij}(q)$ for system A at concentration $x = 0.5$ and total density $\rho R_{11}^3 = 1.49$. The circles are MC simulation results, the solid lines DFT test-particle results and the dotted lines results from using the RPA closure to the OZ equations.

ture factors $S_{11}(q)$ and $S_{22}(q)$ at $q = 0$, indicating that the state point for which these results are calculated is not too far from the spinodal. System A exhibits bulk fluid-fluid phase separation – i.e. we find a solution to the equation $D(q = 0) = 0$, the spinodal for this system. In Fig. 5 we display both the spinodal and the binodal for system A. These are located at rather high (monomer) densities. For example, for $x = 0.5$ the spinodal is located at a monomer density of $\sigma^3 \rho_m = 0.47$, where σ is the monomer diameter. At such densities the reliability of the effective pair potential for dendrimers is perhaps questionable. However, the influence of the macro-phase separation is observable at lower densities,

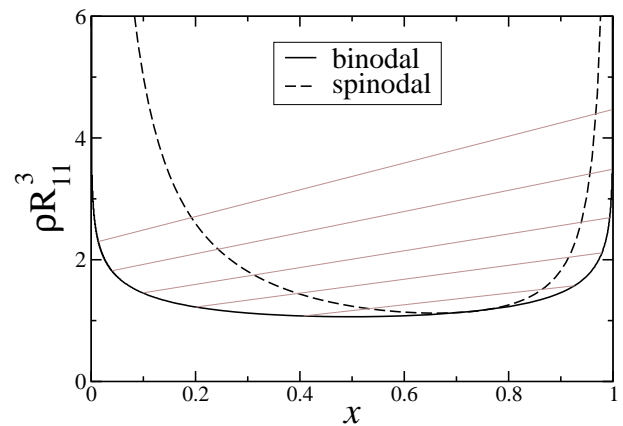


FIG. 5: Phase diagram for the binary dendrimer mixture exhibiting bulk fluid-fluid phase separation (system A), plotted in the total density, ρR_{11}^3 , versus concentration, $x = \rho_2^b / \rho$ plane. The straight lines are the tielines linking coexisting state points on the binodal.

where the structure factors display a local maximum at $q = 0$ – see Fig. 4.

B. Micro-phase separation

The second Gaussian mixture for which we display results, ‘system B’, is a binary mixture of G3 dendrimers with thread length $\delta = 2.0\sigma$ (species 1) and G4 dendrimers with $\delta = 4.7\sigma$ (species 2). Here, the 1-1 interaction is very soft and long ranged, whereas the 2-2 potential is comparatively strong and short ranged. The parameters in the effective pair potentials [Eq. (1)], obtained from MC simulations are:

$$\begin{aligned} \epsilon_{11} &= 6.3 k_B T, & R_{11} &= \sqrt{21}\sigma \\ \epsilon_{22} &= 3.1 k_B T, & R_{22} &= \sqrt{100}\sigma \\ \epsilon_{12} &= 3.2 k_B T, & R_{12} &= \sqrt{52}\sigma. \end{aligned}$$

The pair potentials with these parameters are plotted in Fig. 2. The radial distribution functions $g_{ij}(r)$ for system B are displayed in Fig. 6 for the total bulk density $\rho R_{11}^3 = 0.96$ and concentration $x = 0.5$. We plot MC simulation results, results obtained by inserting the RPA closure into the OZ equations and those from using the RPA DFT via the test-particle route. We find good agreement between the MC and DFT results. The functions $g_{ij}(r)$ decay rather slowly in an oscillatory manner, with wavelength $\lambda \simeq 2R_{22}$. The presence of slowly decaying oscillations indicates that this state point is not too far in the phase diagram from the λ -line. In fact, it turns out that the density $\rho R_{11}^3 = 0.96$, corresponds, at $x = 0.5$, to $0.76\rho_\lambda(x = 0.5)$, where $\rho_\lambda(x)$ is the x -dependent value of the total density on the λ -line. Moreover, the fact that $g_{22}(0) > 1$ indicates that the dendrimers of species 2 prefer complete overlap, a further

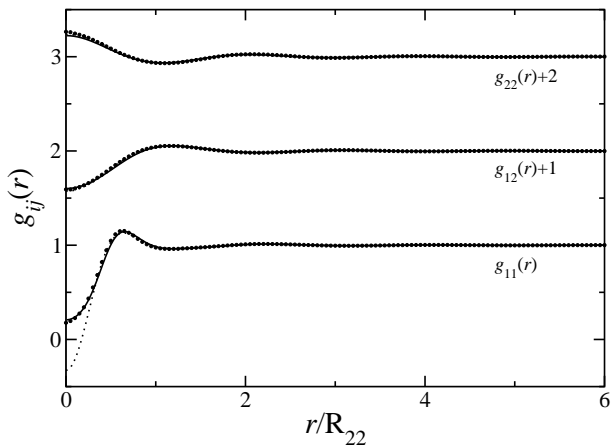


FIG. 6: Partial radial distribution functions $g_{ij}(r)$ for system B with a total density $\rho R_{11}^3 = 0.96$ and concentration $x = 0.5$. The circles are MC simulation results, the solid lines DFT test-particle results and the dotted lines results from the RPA closure to the OZ equations.

indication of the propensity towards microphase ordering; recall the potential $V_{22}(r)$ is purely repulsive.

In Fig. 7 we display the partial structure factors $S_{ij}(q)$ for system B at the state point corresponding to the results displayed in Fig. 6. There is good agreement between the MC simulation results and the DFT results. We see a peak in the structure factors $S_{11}(q)$ and $S_{22}(q)$ at $q = q_c \simeq 3.5R_{22}^{-1}$, indicating the propensity towards micro-phase ordering. System B exhibits a λ -line, i.e., we find a solution to the equation $D(q = q_c > 0) = 0$. In Fig. 8(a) we display the λ -line for system B and in Fig. 8(b) the wavelength λ_c of the instability, $\lambda_c = 2\pi/q_c$, for the points along the λ -line. The λ -line is located at rather high densities: its minimum density $\rho R_{11}^3 = 1.23$ corresponds to a monomer density of $\sigma^3 \rho_m = 0.63$. The length scale of the instability, λ_c , is somewhat smaller than $2R_{22}$ and is rather insensitive to the precise location on the instability line. This indicates that the length scale of the λ -line instability is mainly determined by the larger particles, whose size and interaction range is indeed R_{22} . However, it must be emphasized that the emergence of this inherent instability is a characteristic of the *whole mixture* and it requires the presence of both species with the associated interactions between like and unlike species.

V. CONFINED SYSTEMS

We determine the inhomogeneous fluid density profiles of systems A and B, from the previous section, when these binary dendrimer mixtures are confined in a spherical cavity. Much is known about the behavior of Gaussian mixtures at planar walls²⁵ and in spherical cavities.^{28,29} However, this previous work relied (essen-

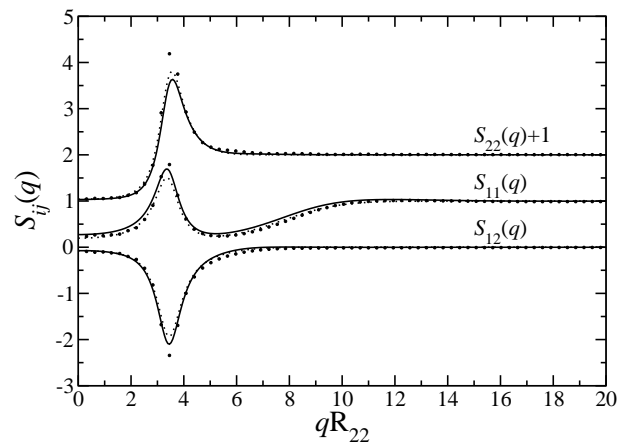


FIG. 7: Partial structure factors $S_{ij}(q)$ for system B at concentration $x = 0.5$ and total density $\rho R_{11}^3 = 0.96$. The circles are MC simulation results, the solid lines DFT test-particle results and the dotted lines results from using the RPA closure to the OZ equations.

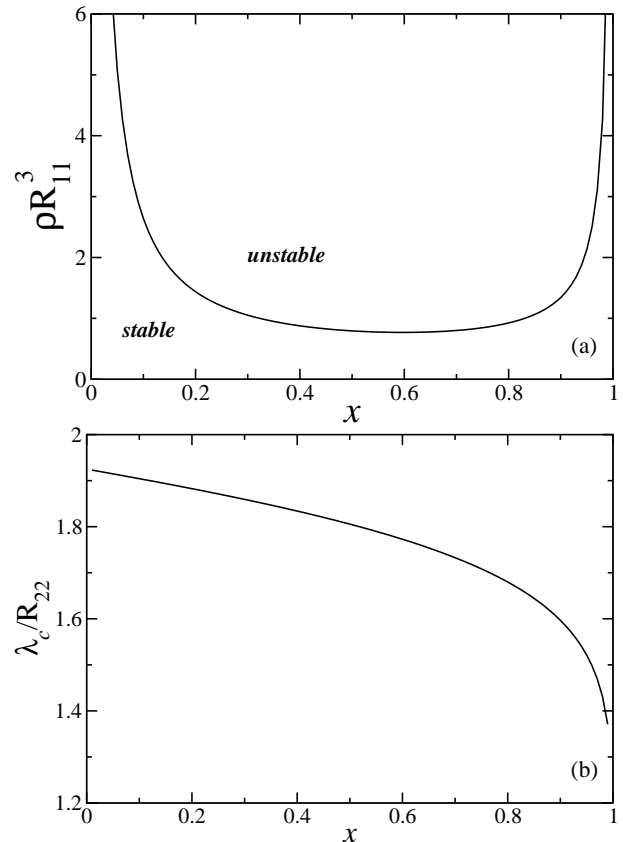


FIG. 8: (a) Stability ‘phase diagram’ for the binary dendrimer mixture exhibiting micro-phase separation, plotted in the total density, ρR_{11}^3 , versus concentration, $x = \rho_2^b/\rho$ plane. The solid line is the λ -line. (b) The wavelength $\lambda_c = (2\pi)/q_c$ of the instability on the λ -line, where q_c is the wavenumber for which $D(q_c) = 0$.

tially) on a guess for the form of the external potentials. Here, we determine effective external potentials between the dendrimers and the wall explicitly. The potential between the individual dendrimer monomers and the cavity wall is assumed to be a hard interaction (i.e. the potential of the monomer is zero inside the cavity and infinite outside the cavity). We calculate an effective potential between the centre of mass of the dendrimers and the wall in a manner similar to that used to derive the dendrimer-dendrimer effective pair potentials – i.e. we perform biased MC simulations of a single monomer-resolved dendrimer near a planar wall where the potential of the monomer is zero for $z > 0$ (z is the Cartesian axis perpendicular to the wall) and infinite for $z < 0$. This planar effective wall potential has the following Yukawa form:

$$V_i^{\text{ext}}(z) = \begin{cases} \frac{\epsilon_i R_{11} \exp[-z/R_i]}{z} & \text{for } z > 0 \\ \infty & \text{otherwise.} \end{cases} \quad (12)$$

For mixture A, the parameters are $\epsilon_1 = 150k_B T$, $R_1 = 0.34R_{11}$, $\epsilon_2 = 70k_B T$ and $R_2 = 0.39R_{11}$. For mixture B, the parameters are $\epsilon_1 = 68k_B T$, $R_1 = 0.39R_{11}$, $\epsilon_2 = 150k_B T$ and $R_2 = 0.89R_{11}$. From Eq. (12) we may then construct the external potential corresponding to a spherical cavity of radius R_{wall} :

$$V_i^{\text{ext}}(r) = \begin{cases} \frac{\epsilon_i R_{11} \exp[-(R_{\text{wall}}-r)/R_i]}{(R_{\text{wall}}-r)} & \text{for } r < R_{\text{wall}} \\ \infty & \text{otherwise.} \end{cases} \quad (13)$$

Of course, this will only provide a reliable approximation to the cavity potential when $R_{\text{wall}} \gg R_{ij}$.

In Fig. 9 we display the fluid density profiles for system A with $N_1 = 15000$ particles of species 1 and $N_2 = 15000$ particles of species 2 confined in a cavity with $R_{\text{wall}}/R_{11} = 12.2$. The average total density in the cavity corresponds to a state point well inside the fluid-fluid demixing binodal. This phase separation is manifest in the fluid one body density profiles. There is preferential adsorption of species 1 at the walls of the cavity and there are almost exclusively just particles of species 2 for $r \lesssim 8R_{11}$, in the centre of the cavity. Which of the two species is preferentially adsorbed by the cavity walls is a rather fine balance, determined by an interplay of the various external wall potential parameters. Slightly changing one of these parameters can lead to adsorption of the other species at the wall.

In Fig. 10 we display the fluid density profiles for system B with $N_1 = 15000$ particles of species 1 and $N_2 = 15000$ particles of species 2 confined in a cavity with $R_{\text{wall}}/R_{22} = 7.2$. The average total density in the cavity corresponds to a state point inside the λ -line. As a consequence, we see rather striking ‘onion-like’ ordering in the cavity – alternating layers rich in the two different species of particles. The DFT and MC simulation results agree well; the DFT is able to capture the details of the highly structured profiles, although a slight phase shift in the oscillations in the profiles is noticeable. This ordering has its origins in the existence of the inherent λ -line

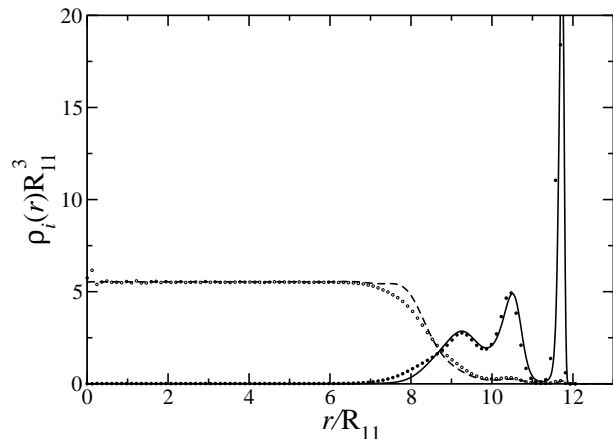


FIG. 9: Density profiles for system A with $N_1 = 15000$ particles of species 1 and $N_2 = 15000$ particles of species 2 confined in a cavity of radius $R_{\text{wall}}/R_{11} = 12.2$. The solid line is the DFT result for species 1 and the dashed line species 2. The symbols are MC simulation results.

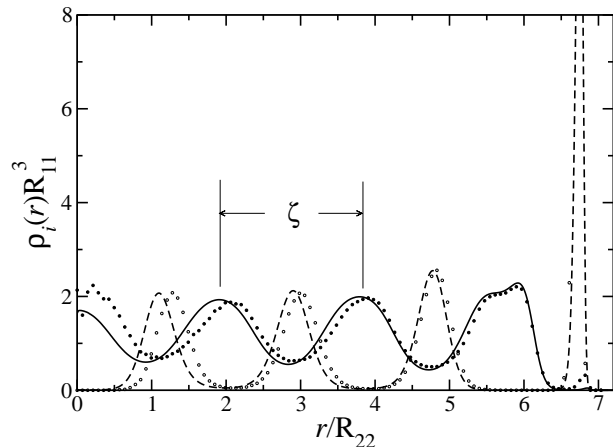


FIG. 10: Density profiles for system B with $N_1 = 15000$ particles of species 1 and $N_2 = 15000$ particles of species 2 confined in a cavity of radius $R_{\text{wall}}/R_{22} = 7.2$. The solid line is the DFT result for species 1 and the dashed line species 2. The symbols are MC simulation results.

instability of the bulk system. Indeed, as can be seen in Fig. 10, the length scale ζ that characterizes the onion structure is roughly $\zeta \cong 2R_{22}$, precisely as the critical wavelength λ_c shown in Fig. 8(b). Under planar confinement, mixture B would have formed alternating layers of species 1-rich and species 1-poor lamellae instead.²¹

VI. CONCLUSIONS

We have investigated mixtures of dendrimers, finding either bulk fluid-fluid demixing or micro-phase separation, depending on the choice of the dendrimers’ genera-

tion numbers and architecture. Here, in contrast to previous studies concerning micro-phase separation, we do *not* employ arbitrary Gaussian potentials but those obtained from monomer-resolved simulations of dendrimers. Furthermore, we observe pattern formation under confinement, finding a strong sensitivity with respect to the form of the wall potential. This work demonstrates, therefore, that the rich phenomenology encountered in Gaussian mixtures can be realized by employing dendrimers as soft colloids with tunable repulsions. It would be desirable to synthesize suitable mixtures of dendrimers, along the lines put forward in this work, with an inherent λ -type instability. Under planar confinement, these would organize in lamellae, which opens the possibility of using dendrimers as lubrication agents, for instance. Another very interesting question is the nature of the phase or phases

that form inside the unstable region enclosed by the λ -line. A rich variety of one-, two-, or three-dimensionally modulated structures (cylinders, lamellae, crystals), similar to that encountered in block copolymer blends or in ternary oil/water/surfactant mixtures could be expected here as well. We plan to return to this problem in the future.

Acknowledgments

This work was funded in part by the Deutsche Forschungsgemeinschaft (DFG). A.J.A. acknowledges the support of EPSRC under Grant No. GR/S28631/01.

-
- ¹ G. R. Newcome, C. N. Moorefield, and F. Vögtle, *Dendritic Molecules: Concepts, Synthesis, Perspectives* (Wiley-VCH: Weinheim 1996).
- ² M. Fischer and F. Vögtle, *Angew. Chem. Int. Ed.* **38**, 884 (1999).
- ³ A. W. Bosman, H. M. Janssen, and E. W. Meijer, *Chem. Rev.* **99**, 1665 (1999).
- ⁴ *Dendrimers and Other Dendritic Polymers*, ed. by J. M. J. Fréchet and D. A. Tomalia (Wiley-VCH: Weinheim 2001).
- ⁵ M. Ballauff and C. N. Likos, *Angew. Chem. Int. Ed.* **43**, 2998 (2004).
- ⁶ I. Lee, B. T. Athey, A. W. Wetzel, W. Meixner, and J. R. Baker, *Macromolecules* **35**, 4510 (2002).
- ⁷ U. Boas and P. M. H. Heegaard, *Chem. Soc. Rev.* **33**, 43 (2004).
- ⁸ A. Quintana, E. Raczka, L. Piehler, I. Lee, A. Myc, I. Majoros, A. K. Patri, T. Thomas, J. Mule, and J. R. Baker, *Pharm. Res.* **19**, 1310 (2002).
- ⁹ P. Kolhe, E. Misra, R.M. Kannan, S. Kannan, and M. Lieh-Lai, *Int. J. Pharm.* **259**, 143 (2003).
- ¹⁰ Y. Choi and J. R. Baker, *Cell Cycle* **4**, 669-671 (2005).
- ¹¹ A. Adronov and J. M. J. Fréchet, *Chem. Commun.* **18**, 1701 (2000).
- ¹² I. Gössl, L. Shu, A. D. Schlüter, and J. P. Rabe, *J. Am. Chem. Soc.* **124**, 6860 (2002).
- ¹³ C. N. Likos, *Phys. Rep.* **348**, 267 (2001).
- ¹⁴ I. O. Götze, H. M. Harreis and C. N. Likos, *J. Chem. Phys.*, **120**, 7761 (2004).
- ¹⁵ C. N. Likos, S. Rosenfeldt, N. Dingenouts, M. Ballauff, P. Lindner, N. Werner, and F. Vögtle, *J. Chem. Phys.* **117**, 1869 (2002).
- ¹⁶ I. O. Götze and C. N. Likos, *Macromolecules* **36**, 8189 (2003).
- ¹⁷ I. O. Götze and C. N. Likos, *J. Phys.: Condens. Matter* **17**, S1777 (2005).
- ¹⁸ A. Lang, C. N. Likos, M. Watzlawek and H. Löwen, *J. Phys.: Condens. Matter* **12**, 5087 (2000).
- ¹⁹ A. A. Louis, P. G. Bolhuis and J.-P. Hansen, *Phys. Rev. E* **62**, 7961 (2000).
- ²⁰ A. J. Archer and R. Evans, *Phys. Rev. E* **64**, 041501 (2001).
- ²¹ A. J. Archer, C. N. Likos and R. Evans, *J. Phys.: Condens. Matter* **16**, L297 (2004).
- ²² R. P. Sear and W. M. Gelbart, *J. Chem. Phys.* **110**, 4582 (1999).
- ²³ R. Evans, *Adv. Phys.* **28**, 143 (1979); R. Evans, in *Fundamentals of Inhomogeneous Fluids*, ed. by D. Henderson (Dekker, New York, 1992).
- ²⁴ J.-P. Hansen and I. R. MacDonald, *Theory of Simple Liquids*, second edition (Academic: New York, 1986).
- ²⁵ A. J. Archer and R. Evans, *J. Phys.: Condens. Matter* **14**, 1131 (2002).
- ²⁶ C. N. Likos, A. Lang, M. Watzlawek and H. Löwen, *Phys. Rev. E* **63**, 031206 (2001).
- ²⁷ L. Acedo and A. Santos, *Phys. Lett. A* **323**, 427 (2004).
- ²⁸ A. J. Archer, *J. Phys.: Condens. Matter* **17**, 1405 (2005).
- ²⁹ A. J. Archer, *J. Phys.: Condens. Matter* **17**, S3253 (2005).
- ³⁰ C. N. Likos and N. W. Ashcroft, *J. Chem. Phys.* **97**, 9303 (1992).